Hindawi Publishing Corporation
International Journal of Antennas and Propagation
Volume 2014, Article ID 539094, 11 pages
http://dx.doi.org/10.1155/2014/539094

Research Article

Design of Compact 4 × 4 UWB-MIMO Antenna with WLAN Band Rejection

Nguyen Khac Kiem,[1] Huynh Nguyen Bao Phuong,[1] and Dao Ngoc Chien[2]

[1] *Hanoi University of Science and Technology, Hanoi 10000, Vietnam*
[2] *Ministry of Science and Technology, Hanoi 10000, Vietnam*

Correspondence should be addressed to Nguyen Khac Kiem; kiem.nguyenkhac@hust.edu.vn

Received 21 January 2014; Revised 9 June 2014; Accepted 15 June 2014; Published 8 July 2014

Academic Editor: Joonhyuk Kang

A compact 4 × 4 UWB-MIMO antenna with rejected WLAN band employing an electromagnetic bandgap (EBG) structure is presented in this paper. The MIMO antenna is electrically small (60 mm × 60 mm), printed on a FR4_epoxy substrate with the dielectric constant of 4.4 and a thickness of 1.6 mm. A mushroom-like EBG structure is used to reject the WLAN frequency at 5.5 GHz. In order to reduce the mutual coupling of the antenna elements, a stub structure acting as a bandstop filter is inserted to suppress the effect of the surface current between elements of the proposed antenna. The final design of the MIMO antenna satisfies the return loss requirement of less than −10 dB in a bandwidth ranging from 2.73 GHz to 10.68 GHz, which entirely covers UWB frequency band, which is allocated from 3.1 to 10.6 GHz. The antenna also exhibits a WLAN band-notched performance at the frequency band of 5.36–6.34 GHz while the values of all isolation coefficients are below −15 dB and the correlation coefficient of MIMO antenna is less than −28 dB over the UWB range. A good agreement between simulation and measurement is shown in this context.

1. Introduction

Recently, a multi-input multi-output (MIMO) system has been proposed [1, 2]. This system increases channel capacity allowing several users to access to various services at the same time. Since the approval by the Federal Communications Commission (FCC) [3] that the ultrawideband (UWB) technology operates from 3.1 to 10.6 GHz, the technology finds itself in a great number of wireless applications. Furthermore, the UWB technology in combination with MIMO techniques has proven to be a solution for the limitation of short-range communications, which requires devices to transmit extremely low power [4]. In such a system, its antennas are designed to ensure that the isolation among their elements should be less than −15 dB. One solution to this problem is that antenna elements are placed apart from the others by at least half a wavelength of the lowest operating frequency; however, this leads to an increase in dimensions of MIMO antennas. Therefore, antenna dimensions and its isolation coefficients are two major criteria to consider in the MIMO antenna design.

In order to reduce mutual coupling between MIMO antennas while maintaining their small electrical length, different approaches have been introduced in numerous design [4–8]. In [4], an inverted Y-shaped stub is inserted into the ground plane between two elements of a UWB-MIMO antenna. Two novel bent slits are etched into the ground plane in [7]. At lower frequencies, the bent slits reduce the mutual coupling and have a slight effect on the reflection coefficient. At higher frequencies, the slits work as slit antennas, widening the impedance bandwidth because the two slits are coupled fed by two 50 Ohm microstrip lines, respectively. Two triangles are cut from the ground plane. In this way, the reflection coefficient and isolation of the two slit antennas can be improved. Moreover, in order to enhance isolation and increase impedance bandwidth, two long protruding ground stubs are added to the ground plane on the other side and a short ground strip is used to connect the ground planes of the two planar monopoles together to form a common ground in [8].

The majority of those antennas are 2 × 2 MIMO-UWB antenna [4, 7, 8] which has not enhanced so much the quality

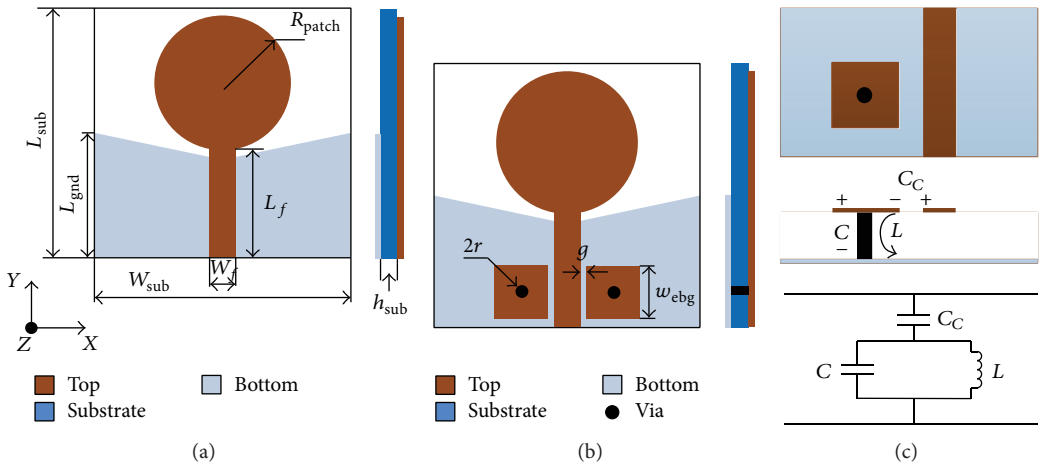

Figure 1: Proposed UWB antenna (a) without EBG structures and (b) with EBG structures and (c) equivalent circuit of WLAN notched based on EBG structures.

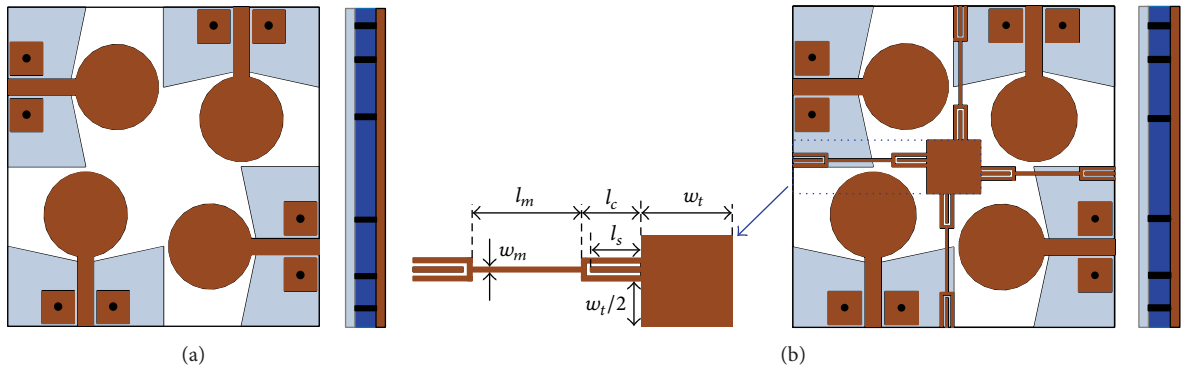

Figure 2: Proposed MIMO antenna: (a) initial MIMO antenna and (b) final MIMO antenna with MMR stub structure. Detailed dimensions in mm: $l_m = 12$, $w_m = 0.5$, $l_c = 6.5$, $l_s = 5.5$, and $w_t = 10$.

of the communication channels. In addition, some designs were not able to operate in the entire UWB band allocated by the FCC [9–12]. On the other hand, a four-element MIMO antenna with better isolation by introducing discontinuities between elements and the system ground plane was presented in [5]. The obtained results show isolation lower than 20 dB. However, the system only works over the frequency range of 2.0–6.0 GHz.

In this paper, a compact 4 × 4 MIMO-UWB antenna with WLAN-notched characteristic is presented. The proposed antenna shows isolation less than −15 dB over its ultrawide operating frequency band ranging from 2.73 to 10.68 GHz and a rejection at the WLAN band of 5.36–6.04 GHz. The unique feature of this design is that the mutual coupling can be reduced by adjusting the length of MMR stub corresponding to a quarter wavelength of frequency which provides the lowest coupling coefficient. Moreover, the notched band based on EBG structures helps to maintain the same radiation patterns at higher frequency rather than using slots cut on the patches [13].

The rest part of this paper is organized as follows. In Section 2, detailed designs of the UWB antennas without and

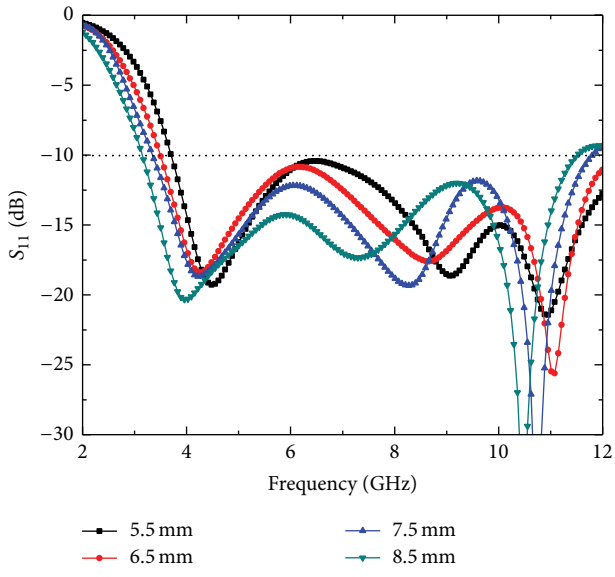

Figure 3: Simulated S_{11} of the single UWB antenna without EBG structures for different parameters of R_{patch}.

Table 1: Design specifications for UWB antennas.

Antenna type	Design parameters (mm)
UWB antenna without EBGs	$L_{sub} = 30$, $W_{sub} = 30$, $W_f = 3$, $R_{patch} = 8$, $L_f = 13$, $L_{gnd} = 15$
UWB antenna with EBGs	$L_{sub} = 30$, $W_{sub} = 30$, $W_f = 3$, $R_{patch} = 8$, $L_f = 13$, $L_{gnd} = 15$, $w_{ebg} = 6.2$, $g = 0.7$, $r = 0.5$

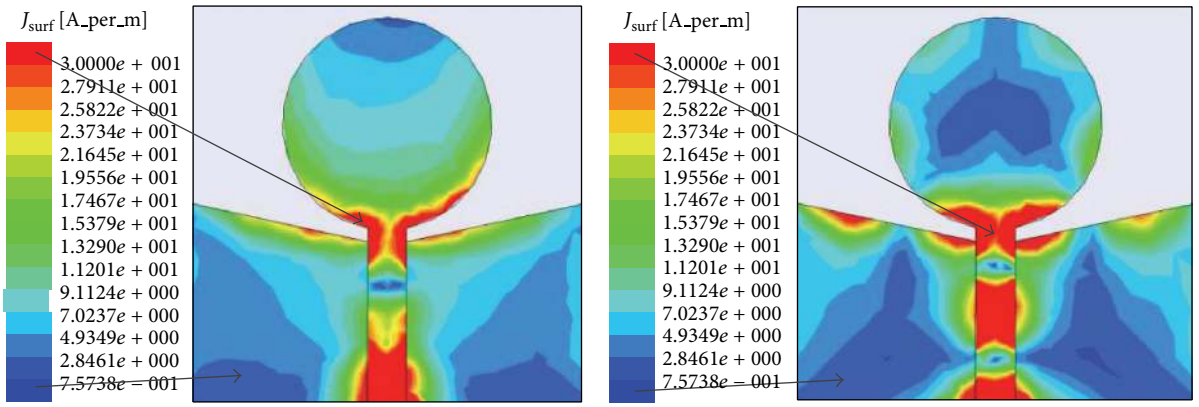

Figure 4: Current distribution on single UWB antenna without EBGs at (a) 4 GHz and (b) 9 GHz.

with EBGs are presented. The proposed MIMO antenna is then introduced in both cases of initial and final design. The simulated and measured results are shown in Section 3, while some conclusions are provided in Section 4.

2. Design of 4 × 4 MIMO-UWB Antenna

In this work, the design of the antenna is divided into two parts. In the first part, an antenna is designed for UWB frequencies ranging from 3.1 GHz to 10.6 GHz. Afterwards, this antenna is integrated with the mushroom-like EBG structure to provide WLAN band-notched characteristic. In the second part, the four notched single antennas are utilized as elements to form a 4 × 4 MIMO antenna. Finally, the stub structure is implemented to diminish the mutual coupling of the antennas.

2.1. Design of UWB Antenna. The two configurations of UWB antenna without and with EBG elements are shown in Figures 1(a) and 1(b), respectively. The antenna consists of a circular radiating patch excited by a 50 Ω microstrip feed line (W_f = 3 mm). On the other side of the substrate, the ground plane with a length of L_{gnd} covers the section of the microstrip fed line. The antennas are printed on a FR4_epoxy substrate with the dielectric constant of 4.4 and a thickness of 1.6 mm.

The antenna integrated with EBG structures is shown in Figure 1(b). Here, the microstrip feed line is placed between two pairs of EBG cells, which are designed to act as stopband filters. With the intent of prohibiting WLAN frequency band, a pair of EBG cells is inserted rather than only using one cell. The equivalent-circuit model of WLAN notched based on EBG structures also is shown in Figure 1(c). The capacitance C_C denotes the coupling between EBG and microstrip line. The capacitance C is due to the voltage gradient between the patch and ground plane, while the inductance L is generated by the current flowing through the shorting via. Therefore, the center resonant frequency is $f_C = 1/2\pi\sqrt{L(C + C_C)}$ and the width of the stopband increases with the rise of C_C or the decrease of the distance between feed line and EBG cells. The dimensions of the EBG cells, the gap between EBG cells and the microstrip line, are optimized to have band rejection from 5 to 6 GHz corresponding to WLAN frequencies. All the dimensions of these antennas are summarized in Table 1.

2.2. Design of 4 × 4 MIMO-UWB Antenna. In this design, the four UWB antennas with EBG structures are rotated clockwise and placed orthogonally to each other to form the 4 × 4 MIMO antenna which has an overall size of 60 mm × 60 mm. The layout of the MIMO antenna is shown in Figure 2(a).

With the aim of reducing the mutual coupling in the initial MIMO antenna, a stub structure is adopted to form the final antenna depicted in Figure 2(b). The design of this structure was based on the principle of the microstrip multimode resonator (MMR) [14, 15]. These stubs are placed between the antennas and connected to each other by a square placed at the center of the MIMO antenna. The mutual coupling between the antennas will be investigated for finding the range of frequency in which the isolation coefficients are not lower than −15 dB. The length l_m of the MMR stub is then set at a value that is approximately equal to a quarter wavelength at the defined frequency.

3. Results and Discussions

This part will discuss the performance of the proposed antennas through both simulation and measurement results.

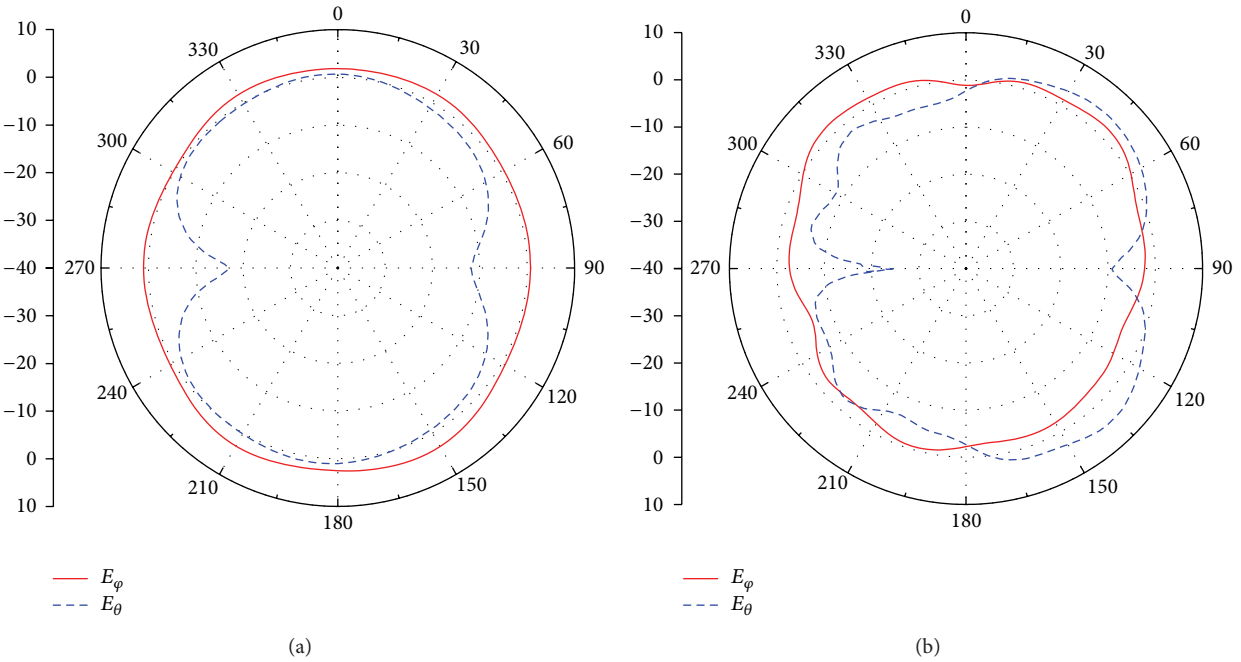

Figure 5: Simulated radiation patterns of the UWB antenna without EBGs in xz-plane at (a) 4 GHz and (b) 9 GHz.

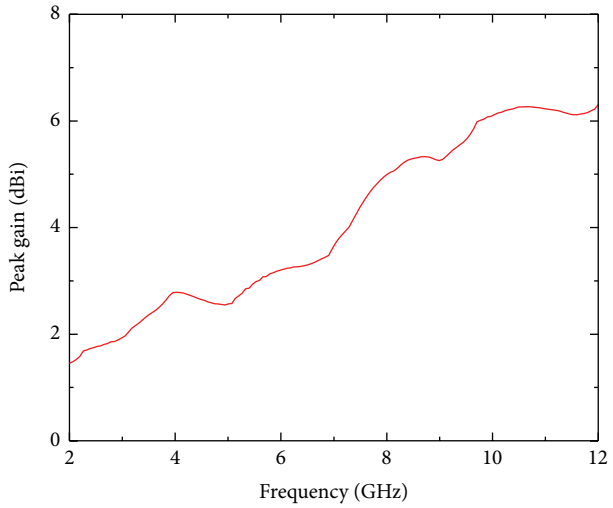

Figure 6: Simulated peak gain of the single UWB antenna without EBGs.

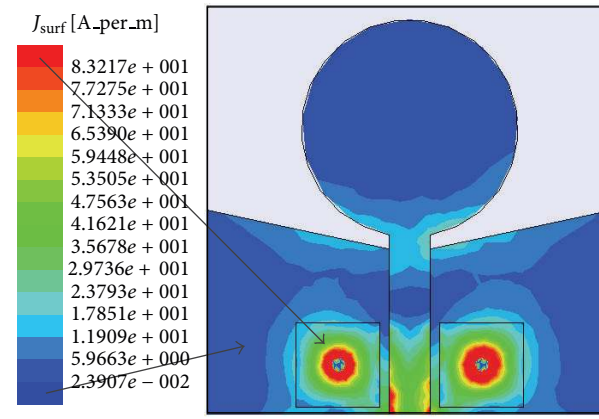

Figure 7: Surface current distribution on UWB antenna with EBG structures at 5.5 GHz.

3.1. UWB Antenna. The simulated S_{11} results of the UWB antenna without EBG structure with different values of R_{patch} are shown in Figure 3. It can be seen that the bandwidth of the antenna defined by the S_{11} less than −10 dB entirely covers the UWB frequency range. The decrease of R_{patch} causes the increase of the impedance mismatching at lower frequency range. The optimized bandwidth is obtained when the R_{patch} is chosen as 8 mm.

Current distributions of the antenna at certain frequencies are exhibited in Figure 4. As observed in Figure 4(a), the current distribution at 4 GHz proves that the antenna operates at its fundamental mode, while the current distribution at 9 GHz in Figure 4(b) indicates the higher resonant mode, which is corresponding to the third order harmonic. Hence, the antenna can work over the broad range of UWB.

Typical radiation patterns of the antenna at 4 GHz and 9 GHz in xz-plane are plotted in Figures 5(a) and 5(b), respectively. The solid lines display the E_φ, and the dotted lines represent E_θ. From Figure 5(a), the antenna possesses a dipole-like radiation pattern confirming its operation in the fundamental resonant mode. The pattern at higher frequency, from Figure 5(b), corresponds to the harmonics of the fundamental resonant mode which are closely spaced [16]. The simulated peak gain of the antenna is depicted in Figure 6, in which the higher frequencies provide larger antenna gain. This is a good agreement with the theory.

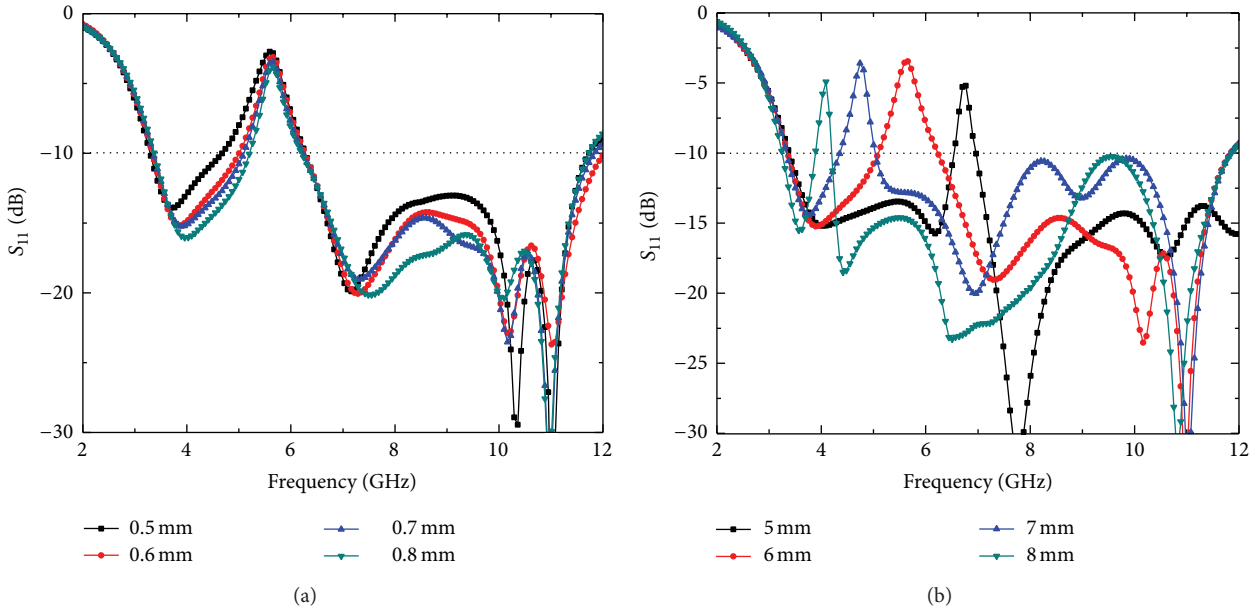

FIGURE 8: Simulated S_{11} of the single UWB antenna integrated with EBG structures for different parameters of (a) g and (b) w_{ebg}.

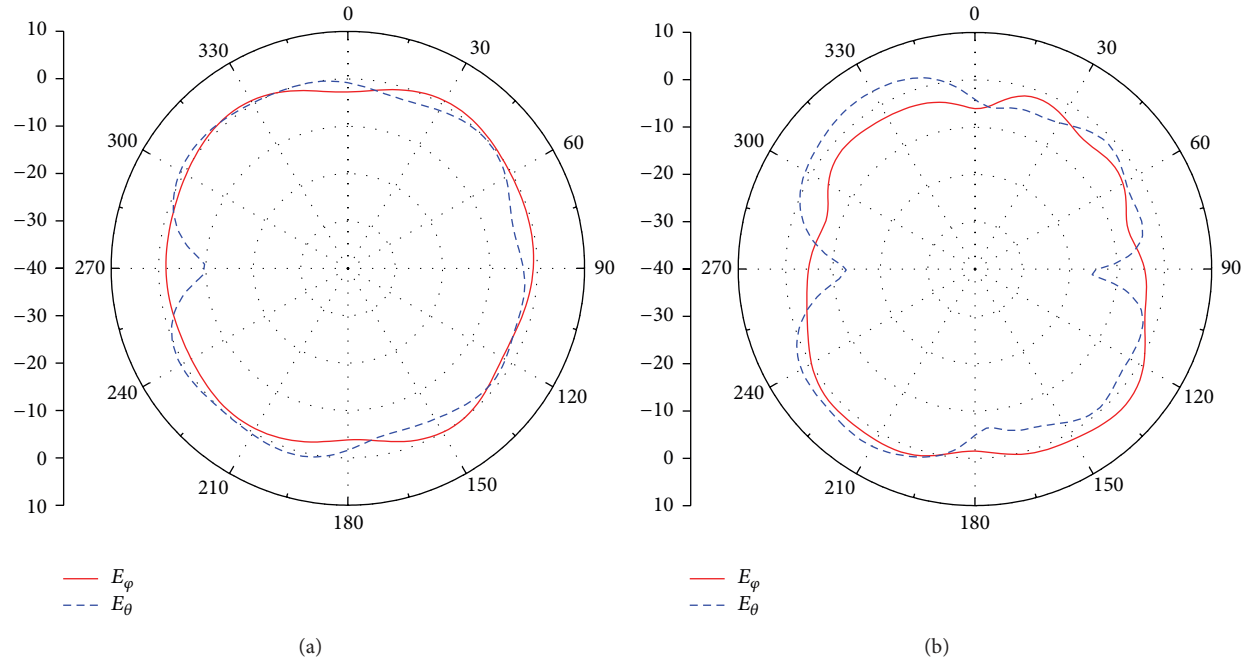

FIGURE 9: Simulated radiation patterns of the UWB antenna integrated with EBGs in xz-plane at (a) 4 GHz and (b) 9 GHz.

The effect of EBG structures on UWB antenna is shown in Figure 7. At the center frequency of WLAN band (5.5 GHz), the current distribution on antenna mainly focuses on the EBG structures, and therefore the patch antenna will not radiate resulting in a notched frequency band.

In order to obtain the desired notched band, parametric studies on the dimension of EBG cell w_{ebg} and the distance g between EBG cells and the feed line are investigated. Figure 8 shows the simulated S_{11} of antenna for different values of the gap g. In Figure 8(a), the width of the notched band reduced when the value of gap g increases, while the simulated S_{11} of antenna for different values of EBG size w_{ebg} is also depicted in Figure 8(b). It should be noticed in Figure 8(b) that the frequency of the notched band also reduces with the increasing value of w_{ebg}. Therefore, the notched-band tuning requires a combination of both values.

Figures 9(a) and 9(b) show the radiation pattern of the proposed UWB antenna at 4 GHz and 9 GHz, respectively.

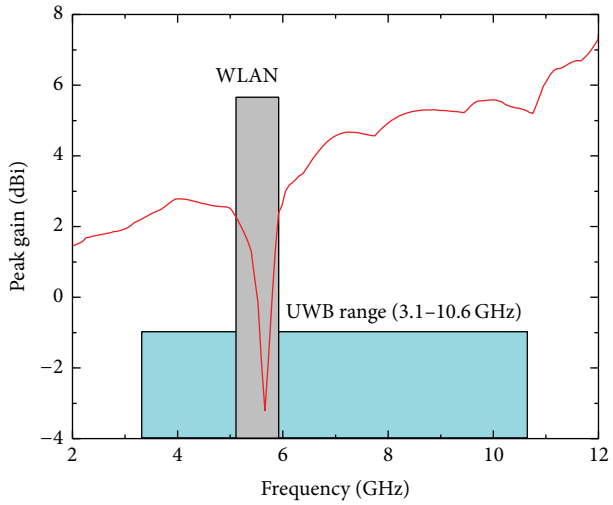

Figure 10: Simulated peak gain of the single UWB antenna integrated EBGs.

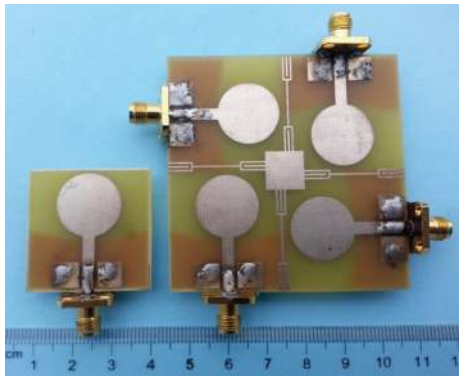

Figure 11: Fabricated UWB integrated EBGs antenna and final MIMO antenna.

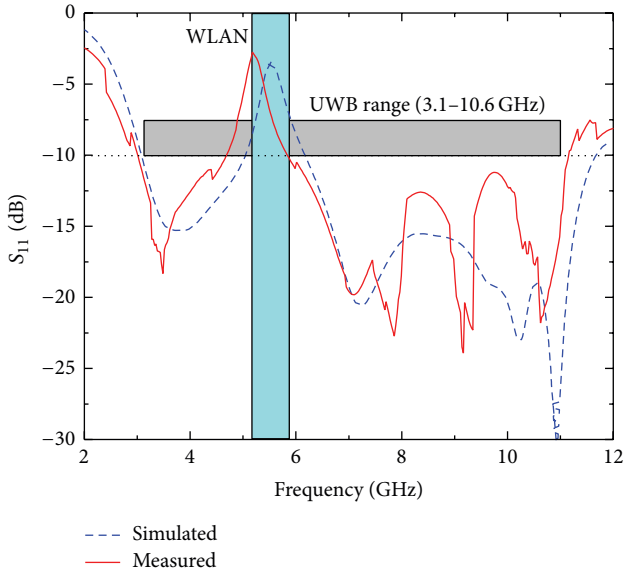

Figure 12: Simulated and measured results of S_{11} of the UWB integrated EBGs with WLAN band notched antenna.

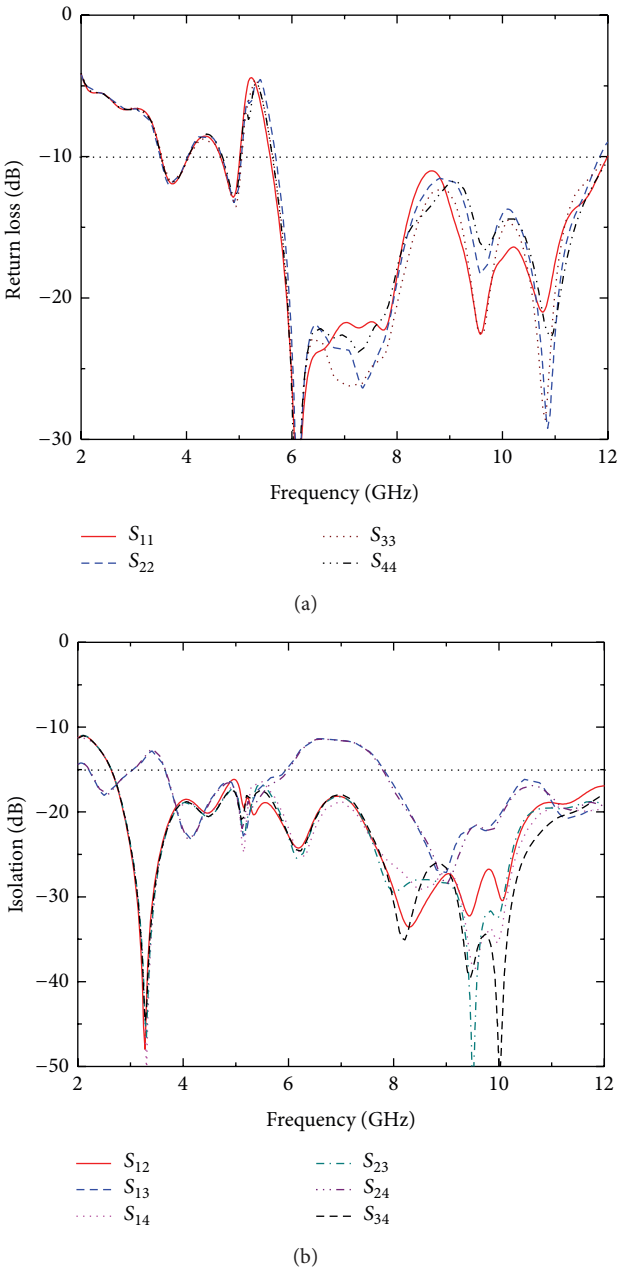

Figure 13: Simulated results of the initial MIMO antenna: (a) return loss and (b) isolation coefficient.

The radiation patterns at high frequency of the antenna with and without EBGs are of small variation due to the lack of etching or cutting on the surface of the patch antenna.

The simulated peak gain versus frequency is shown in Figure 10. It reveals a significant drop in the peak gain within the rejected bands when the antenna employs the EBG cells. A relatively stable peak gain remains over the UWB bandwidth except a 5 dB gain drop in the notched band.

Finally, the fabrication of the proposed antenna is presented in Figure 11. The simulated and measured results of S_{11} of the UWB antenna with EBG cells are shown in Figure 12. From this figure, it is observed that the antenna can operate

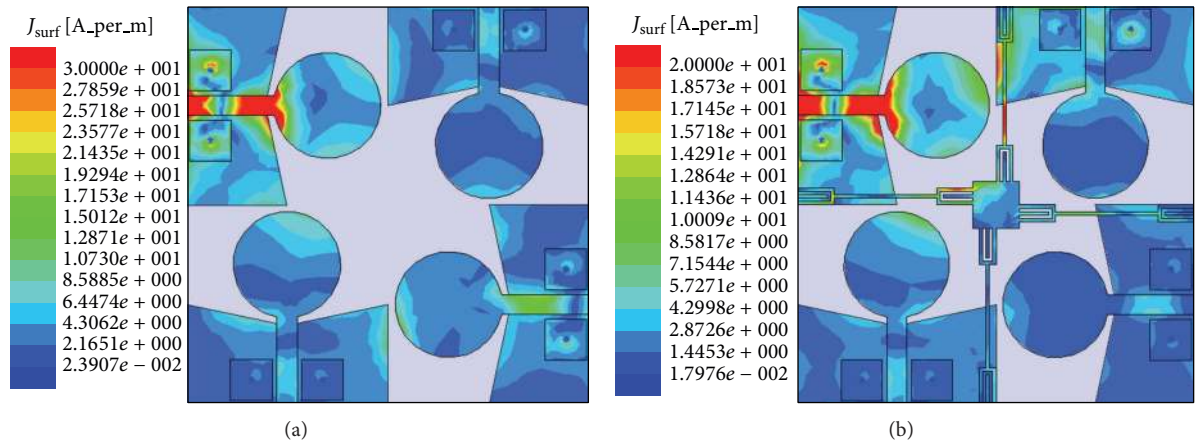

FIGURE 14: Surface current distribution at 6.7 GHz on (a) initial MIMO antenna and (b) final MIMO antenna.

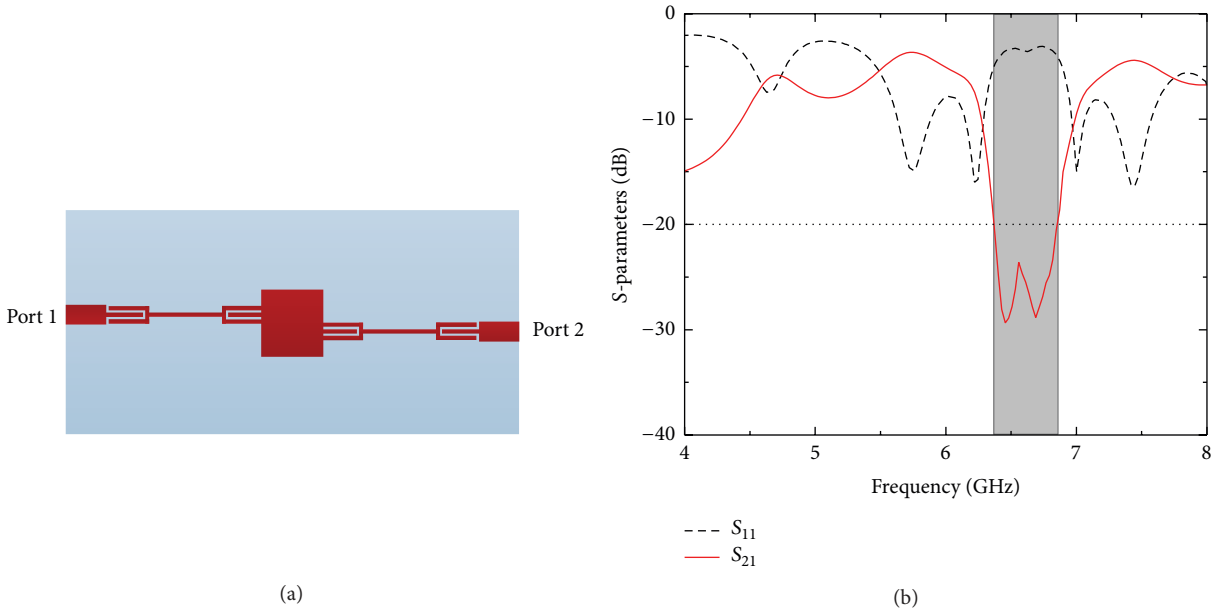

FIGURE 15: (a) Bandstop filter model and (b) simulated S-parameters of the filter.

over the range spreading from 2.98 GHz to 11.16 GHz and exhibits a good rejection at frequencies of WLAN from 4.71 GHz to 5.83 GHz.

3.2. 4 × 4 MIMO-UWB Antenna. The simulated results of reflection coefficients of the initial MIMO antenna are shown in Figure 13(a). As can be seen from Figure 13(a), the reflection coefficients of the antenna do not satisfy impedance matching from 4 to 4.5 GHz. On the other hand, the isolation coefficients between the elements of the initial antenna (see Figure 13(b)) are very low at 6–8 GHz (about −10 dB). This fact is clearly demonstrated by the surface current distribution on the initial antenna in Figure 14(a). As can be observed from Figure 14(a), when the first element is excited, the surface current is strongly induced on the opposite element resulting in a rise of the mutual coupling (S_{13} and S_{24}). Actually, the mutual coupling can be reduced by increasing the distance between the elements. However, this will lead to the larger size of the proposed MIMO antenna.

These drawbacks of the initial MIMO antenna can be solved thanks to the use of stub structure in the final MIMO design. It can be seen from Figure 13(b) that the mutual coupling has a high value at about 6.7 GHz. Therefore, the length l_m of the stub structure is selected as 12 mm, approximately a quarter wavelength at 6.7 GHz. The configuration of this stub is designed based on the principle of MMR structure. Actually, the stub structure acts as a bandstop filter which produced a stopband from 6.35 to 6.87 GHz. Therefore, the filter will suppress the induced currents caused by the copolarization elements at the center frequency of 6.7 GHz. The bandstop filter model and simulated S-parameters of the filter are given in Figures 15(a) and 15(b), respectively.

In Figure 16(a), the bandwidth of the final antenna entirely covers the UWB operating band, whereas the

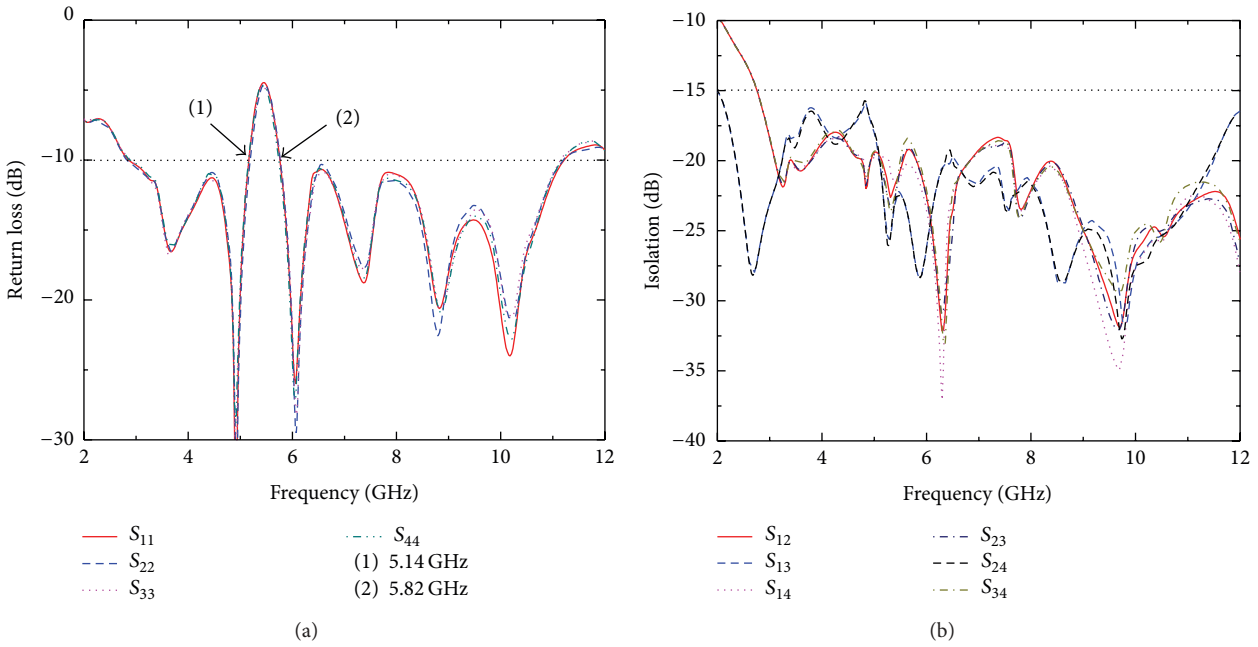

FIGURE 16: Simulated results of the final MIMO antenna: (a) return loss and (b) isolation coefficient.

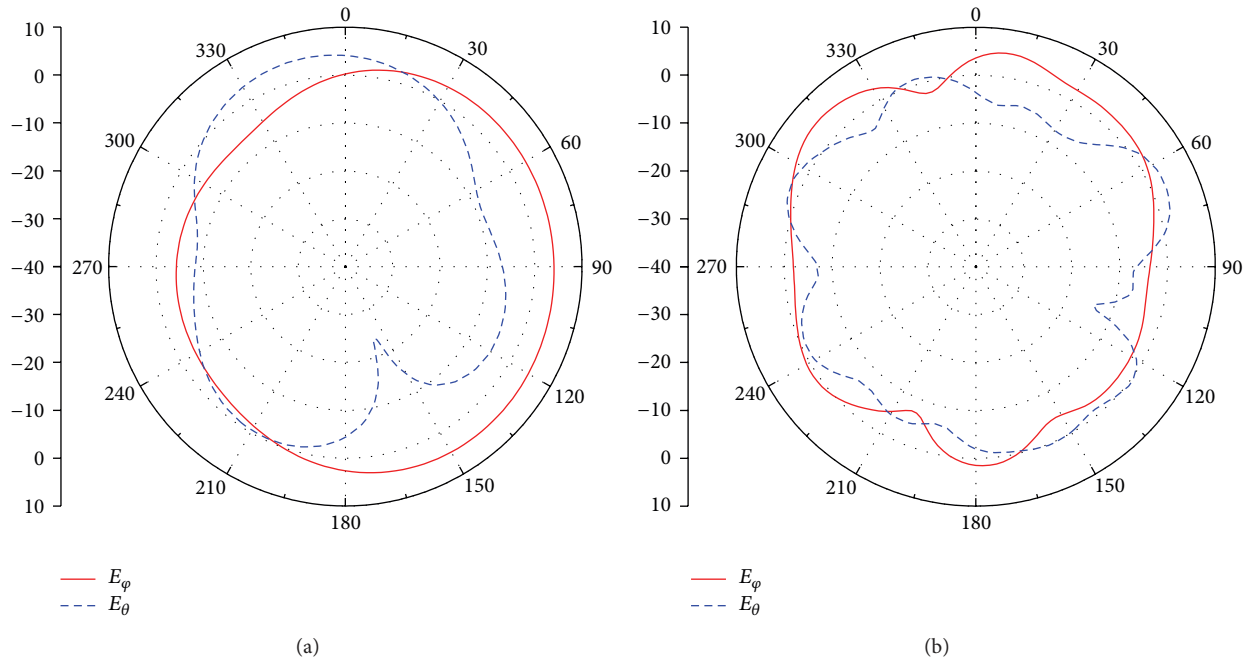

FIGURE 17: Simulated radiation patterns of the initial MIMO antenna in xz-plane at (a) 4 GHz and (b) 9 GHz.

notched band appears in WLAN range (from 5.14 to 5.82 GHz). Moreover, in Figure 16(b), the mutual coupling between the opposite-side elements decreases to below −15 dB. The current distribution of the final antenna at 6.7 GHz is focused on the stub structures shown in Figure 14(b). Therefore, the effect of the surface current on the copolarization element is reduced.

Figures 17 and 18 show the simulated radiation patterns of initial and final MIMO antenna, respectively. From these figures, the radiation patterns of both antennas at lower frequency (4 GHz) are directional, while nearly omnidirectional patterns are observed at higher frequency (9 GHz). The simulated peak gain of final MIMO antenna is presented in Figure 19. The stable gain is maintained over the UWB range

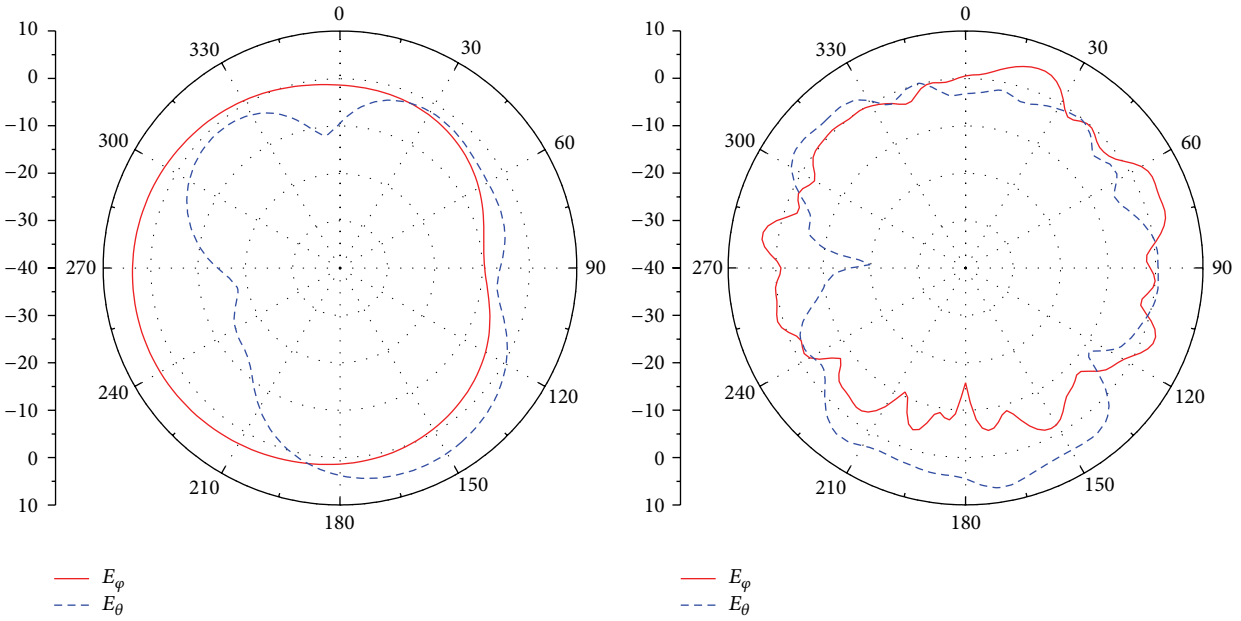

Figure 18: Simulated radiation patterns of the final MIMO antenna in xz-plane at (a) 4 GHz and (b) 9 GHz.

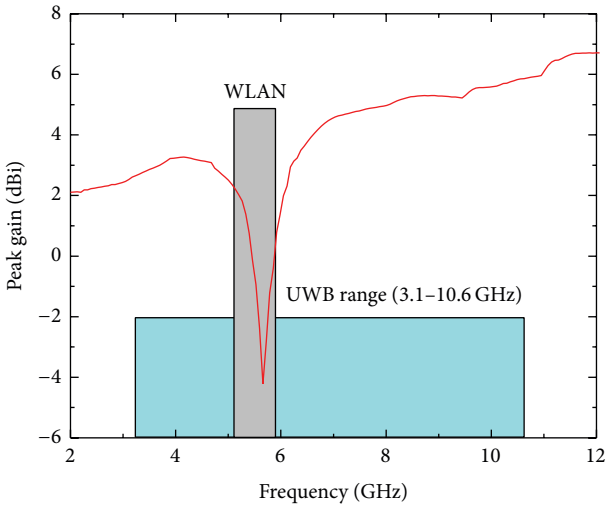

Figure 19: Simulated peak gain of the final MIMO antenna.

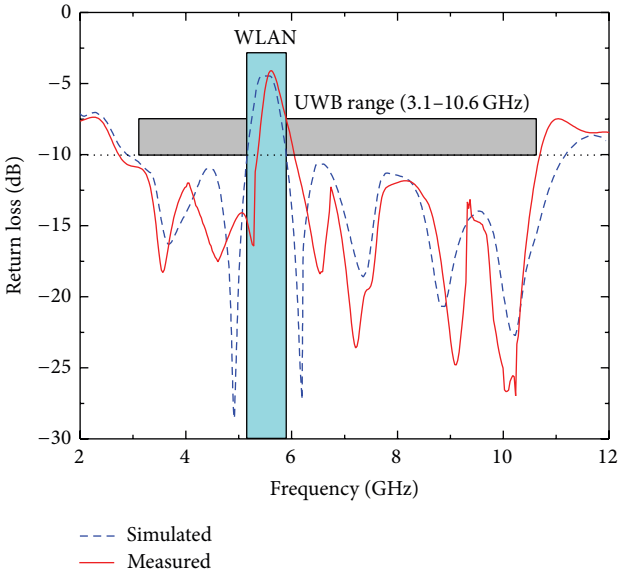

Figure 20: Simulated and measured results of return loss of the final MIMO antenna.

while a gain drop of 4.5 dB is observed at the WLAN-notched band.

Figure 20 presents the measured return loss of the fabricated final MIMO antenna shown in Figure 11. It works well over a broad range of frequenciesfrom 2.73 to 10.68 GHz and possesses a rejected band at the WLAN band from 5.36 to 6.04 GHz. Meanwhile, Figure 21 shows the results of mutual coupling of the cross- and copolarization elements of the final MIMO antenna. The measured results show that the mutual coupling between cross- (S_{12}) and copolarization elements (S_{13}) is less than −17 dB and −16 dB over UWB range, respectively. It should be noted that the measured results are in a good agreement with the simulated results.

3.3. MIMO Characteristics. It is required that MIMO antennas must be characterized for their diversity performance. In a diversity system, the signals are usually correlated due to the distance between the antenna elements [4]. The parameter used to assess the correlation between radiation patterns is the envelope correlation coefficient. It is required to minimize

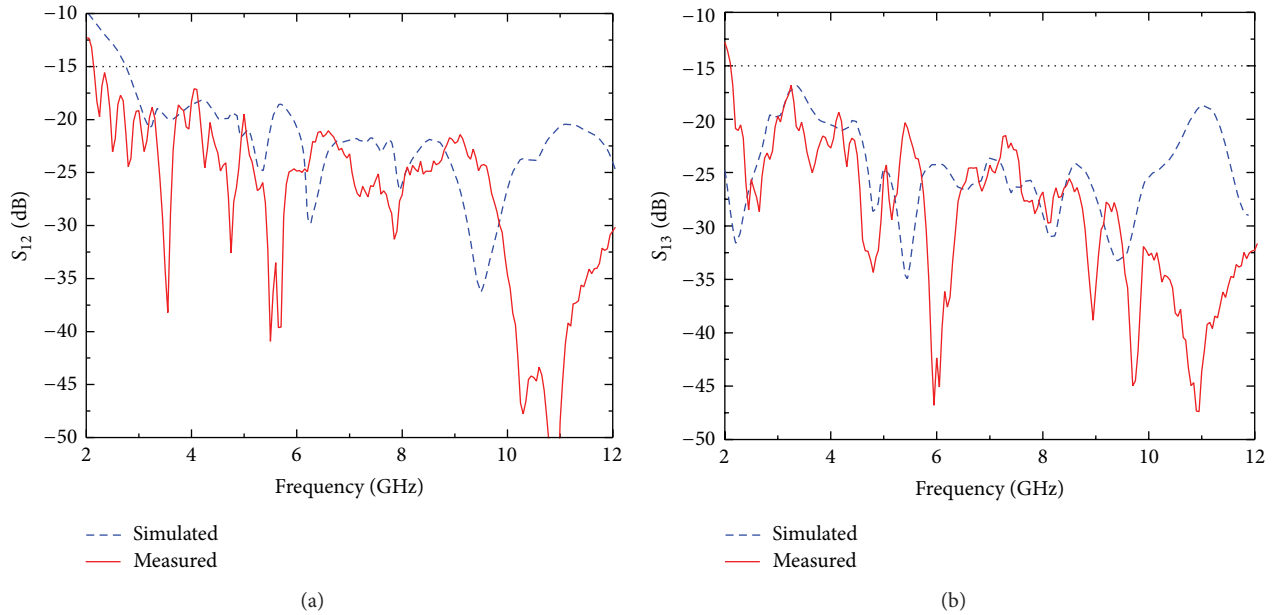

FIGURE 21: Simulated and measured results of mutual coupling of the final MIMO antenna: (a) cross-polarization elements and (b) copolarization elements.

the correlation because the relationship of the correlation with diversity gain is that the lower is the correlation, the higher will be the diversity gain and vice versa. Normally, the value of the envelope correlation at a certain frequency is small in case that the radiation patterns of one antenna are different from each other. Otherwise, the same patterns of these antennas exhibit the larger value of the envelope correlation.

The correlation coefficient can be calculated from radiation patterns or scattering parameters. Assuming uniform multipath environment, the envelope correlation (ρ_e), simple square of the correlation coefficient (ρ), can be calculated conveniently and quickly from S-parameters [17] as follows:

$$\rho_e(i,j,N) = \frac{\left|\sum_{n=1}^{N} S_{i,n}^{*} S_{n,j}\right|^2}{\prod_{k=(i,j)}\left[1 - \sum_{n=1}^{N} S_{i,n}^{*} S_{n,k}\right]}. \quad (1)$$

Equation (1) depicts the envelope correlation between the antennas i and j in the (N, N) MIMO system. In case of $i = 1$, $j = 2$, and $N = 4$, the envelope correlation of proposed MIMO antenna can be defined as follows:

$$\begin{aligned}\rho_e(1,2,4) &= \left|S_{11}^{*}S_{12} + S_{12}^{*}S_{22} + S_{13}^{*}S_{32} + S_{14}^{*}S_{42}\right|^2 \\ &\times \left(\left[1 - \left(S_{11}^{*}S_{11} + S_{12}^{*}S_{21} + S_{13}^{*}S_{31} + S_{14}^{*}S_{41}\right)\right]\right. \\ &\left.\times \left[1 - \left(S_{11}^{*}S_{12} + S_{12}^{*}S_{22} + S_{13}^{*}S_{32} + S_{14}^{*}S_{42}\right)\right]\right)^{-1}. \end{aligned} \quad (2)$$

The simulated envelope correlation coefficient is shown in Figure 22. From this figure, the proposed MIMO antenna has a minimum correlation coefficient of −56 dB and less than −28 dB over the UWB frequency range. It should be noticed that a very low value of correlation coefficient results in ensured high diversity gain. Therefore, the presented correlation coefficient is suitable for mobile communication with a minimum acceptable correlation coefficient of 0.5 [18].

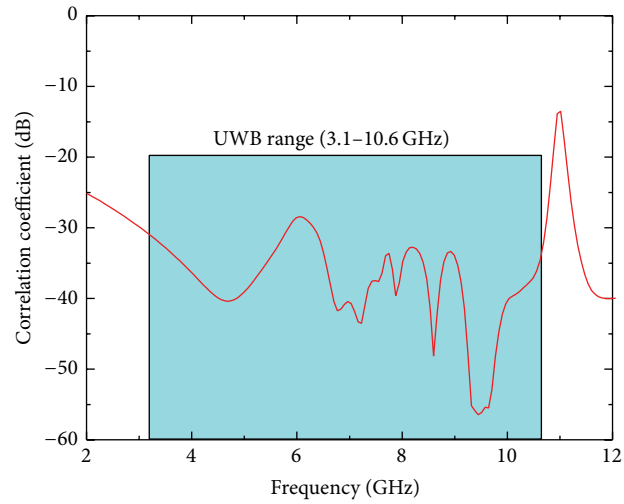

FIGURE 22: Simulated proposed MIMO antenna's envelope correlation coefficient.

The simulated result of group delay of the proposed MIMO antenna is shown in Figure 23. It can be seen that a distortion (≥1 ns) occurred at 5.5 GHz while the other part of operating band keeps relatively flat. The variation of group delay is found to be less than 1 ns showing good phase linearity and thus it fulfills the requirement for UWB operations.

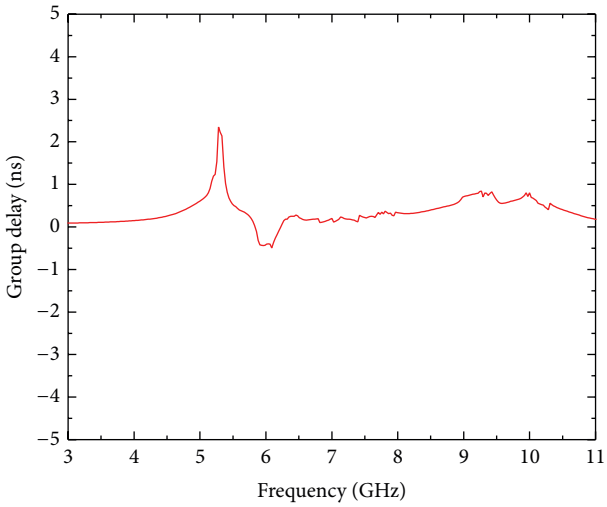

Figure 23: Simulated group delay of proposed MIMO antenna.

4. Conclusions

The compact 4 × 4 MIMO-UWB antenna is designed to operate in ultrawide frequency range with rejected band at WLAN frequency based on EBG structures. The stub structures acting as bandstop filter are inserted to suppress the effect of surface current on the elements of the proposed antenna for reducing the mutual coupling. The fabricated MIMO antenna shows isolation less than −15 dB over its ultrawide operating frequency band spreading from 2.73–10.68 GHz and rejection at the WLAN band of 5.36–6.04 GHz. The proposed MIMO antenna has also a minimum correlation coefficient of −56 dB and less than −28 dB over the UWB frequency range, making it a good candidate for UWB-MIMO applications.

Conflict of Interests

The authors declare that there is no conflict of interests regarding the publication of this paper.

References

[1] G. J. Foschini and M. J. Gans, "On limits of wireless communications in a fading environment when using multiple antennas," *Wireless Personal Communications*, vol. 6, no. 3, pp. 311–335, 1998.

[2] L. Zheng and D. N. C. Tse, "Diversity and multiplexing: a fundamental tradeoff in multiple-antenna channels," *IEEE Transactions on Information Theory*, vol. 49, no. 5, pp. 1073–1096, 2003.

[3] F. C. C. (FCC), "Revision of part 15 of the commissions rules regarding ultra-wideband transmission systems," First Report and Order ET Docket 98-153, FCC 02-48, 2002.

[4] A. Najam, Y. Duroc, and S. Tedjni, "UWB-MIMO antenna with novel stub structure," *Progress In Electromagnetics Research C*, vol. 19, pp. 245–257, 2011.

[5] S.-Y. Lin and H.-R. Huang, "Ultra-wideband MIMO antenna with enhanced isolation," *Microwave and Optical Technology Letters*, vol. 51, no. 2, pp. 570–573, 2009.

[6] S. Zhang, Z. Ying, J. Xiong, and S. He, "Ultrawideband MIMO/diversity antennas with a tree-like structure to enhance wideband isolation," *IEEE Antennas and Wireless Propagation Letters*, vol. 8, pp. 1279–1282, 2009.

[7] J. Li, Q. Chu, and T. Huang, "A compact wideband MIMO antenna with two novel bent slits," *IEEE Transactions on Antennas and Propagation*, vol. 60, no. 2, pp. 482–489, 2012.

[8] L. Liu, S. W. Cheung, and T. I. Yuk, "Compact MIMO antenna for portable devices in UWB applications," *IEEE Transactions on Antennas and Propagation*, vol. 61, no. 8, pp. 4257–4264, 2013.

[9] K. Wong, S. Su, and Y. Kuo, "A printed ultra-wideband diversity monopole antenna," *Microwave and Optical Technology Letters*, vol. 38, no. 4, pp. 257–259, 2003.

[10] T. S. P. See and Z. N. Chen, "An ultrawideband diversity antenna," *IEEE Transactions on Antennas and Propagation*, vol. 57, no. 6, pp. 1597–1605, 2009.

[11] A. Rajagopalan, G. Gupta, A. S. Konanur, B. Hughes, and G. Lazzi, "Increasing channel capacity of an ultrawideband MIMO system using vector antennas," *IEEE Transactions on Antennas and Propagation*, vol. 55, no. 10, pp. 2880–2887, 2007.

[12] S. Zhang, B. K. Lau, A. Sunesson, and S. He, "Closely-packed UWB MIMO/diversity antenna with different patterns and polarizations for USB dongle applications," *IEEE Transactions on Antennas and Propagation*, vol. 60, no. 9, pp. 4372–4380, 2012.

[13] X. L. Liu, Z. D. Wang, Y. Z. Yin, and J. H. Wang, "Closely spaced dual band-notched UWB antenna for MIMO applications," *Progress in Electromagnetic Research C*, vol. 46, pp. 109–116, 2014.

[14] J. W. Baik, S. M. Han, C. Jeong, J. Jeong, and Y. S. Kim, "Compact ultra-wideband bandpass filter with EBG structure," *IEEE Microwave Wireless Components Letter*, vol. 51, pp. 364–370, 2008.

[15] K. Ma, K. Liang, R. M. Jayasuriya, and K. S. Yeo, "A wideband and high rejection multimode bandpass filter using stub perturbation," *IEEE Microwave and Wireless Components Letters*, vol. 19, no. 1, pp. 24–26, 2009.

[16] K. Bahadori and Y. Rahmat-Samii, "A miniaturized elliptic-card UWB antenna with WLAN band rejection for wireless communications," *IEEE Transactions on Antennas and Propagation*, vol. 55, no. 11, pp. 3326–3332, 2007.

[17] J. Thaysen and K. B. Jakobsen, "Envelope correlation in (N, N) mimo antenna array from scattering parameters," *Microwave and Optical Technology Letters*, vol. 48, no. 5, pp. 832–834, 2006.

[18] M. P. Karaboikis, V. C. Papamichael, G. F. Tsachtsiris, C. F. Soras, and V. T. Makios, "Integrating compact printed antennas onto small diversity/MIMO terminals," *IEEE Transactions on Antennas and Propagation*, vol. 56, no. 7, pp. 2067–2078, 2008.